Preparation and characterization of nanoencapsulated synthetic soybean oil derivative-an abundant and environmentally friendly phase change material-heat transfer analysis and applications

Jorge Bergamo[a], Ezequiel Rossi[b,c], Juan Martín Maffi[b,c], Laura De Angelis[b], María Inés Errea[b,*]

[a] Departamento de Ingeniería Química, Facultad Regional Avellaneda, Universidad Tecnológica Nacional, Av. Ramón Franco 5050 (1874), Villa Domínico, Buenos Aires, Argentina
[b] Instituto Tecnológico de Buenos Aires (ITBA), Departamento de Ingeniería Química, Av. Eduardo Madero 399 (1106), Buenos Aires, Argentina
[c] CONICET, Buenos Aires, Argentina

Keywords:
Soybean oil
Environmental friendly phase change material
Thermal energy storage
Abundant and renewable source

The thermal properties of a phase change material (PCM), together with its environmental health risks and natural abundance are important aspects to consider when choosing one for a domestic application. In this work, a soybean oil derivative, which comes from one of the most abundant crops on Earth, is proposed as PCM. A heat transfer model was developed to compare the performance of the proposed PCM, under the same boundary and initial conditions, with other materials reported in literature that have well-known disadvantages in terms of flammability, renewability, abundance and environmental care. Results showed that its performance was as good as theirs. Nanocapsules of the PCM coated with TiO_2 were prepared and characterized physical, thermal and morphologically. Thermal studies were carried out in a device designed and constructed simulating a water heater, and a reduction of about 70% of the PCM phase thermal resistance due to the TiO_2 shell was observed. Furthermore, the calculated thermal energy stored in the device filled with nanoencapsulated PCM was 10.6% higher with respect to the blank, and the total cooling time of the water was increased by over 18% thanks to the PCM.

Introduction

Despite global concerns about the adverse environmental impact caused by fossil fuels, the energy demand is increasing at an average annual rate of approximately 2%, driven by population growth and industrial development [1]. Therefore, it is necessary to encourage the use of renewable energy as well as to implement actions to improve energy efficiency [2–4].

The results are promising and encourage further studies geared towards the implementacion of this system in solar water heaters.

Since most of the total world energy is consumed by households [5], it is essential to develop strategies to reduce this energy demand. Thermal energy storage involving the so-called phase change materials (PCMs), which make use of the energy stored during the melting process [6], is one of the options raised for family energy saving that has aroused more interest in the last decade. In addition to its thermal properties, the availability of a phase change material (PCM), together with its environment and health risks are important aspects to consider when choosing one for a domestic application.

Among organic PCMs, strangely, paraffines are the most popular, despite their flammability and their non-renewable source [7,8]. Conversely, fatty acids, in addition to their low volatility, lack or minimum subcooling, high latent heat, non-flammability and low volume change in phase change, can be obtained from renewable sources and are biodegradable [9]. In recent years there have been several reports proposing pure fatty acids as PCMs [10–16], but none of them explain how they would be obtained for large scale applications. To the best knowledge of the authors, fatty acids are present in nature as mixtures, and the processes required to obtain pure fatty acids from these mixtures are complex and expensive.

Taking into account the above discussion, this paper proposes the use of soybean oil, one of the most abundant crops in the world, as raw material for a novel PCM. Soybean oil is a mixture of triglycerides which on average contains: palmitic (16:0) (11%), stearic (18:O) (4%), oleic (18:1) (23%), linoleic (54%) (18:2), and linolenic (18:3) (8%) acids [17]. This oil is a liquid that, after hydrolysis and hydrogenation gives a solid mixture of stearic and palmitic acid on an average ratio of 89:11.

* Corresponding author.
E-mail address: merrea@itba.edu.ar (M.I. Errea).

Nomenclature

A	Surface (m^2)
C_p	Specific heat capacity (W g^{-1} K^{-1})
$\bar{c}_l$	Function of Pr
$\bar{c}_t$	Function of Pr and geometry
e	Thickness (mm)
$E\%$	Relative error
G	Geometry-dependent constant
g	Acceleration of gravity (m s^{-2})
h	Convective heat transfer coefficient (W m^{-2} K^{-1})
k	Thermal conductivity (W m^{-1} K^{-1})
L	Height (mm)
m	Weight (g)
n	Constant - Exponent used in correlation
Nu	Nusselt number
Nu_{COND}	Conduction Nusselt number
Pr	Prandtl number
Q	Heat (J)
$\dot{Q}$	Heat flux (W)
r	Radius (mm)
R	Thermal Resistance (K W^{-1})
$\%R$	Encapsulation ratio
Ra	Rayleigh number
SD	Standard deviation
t	Time (s)
T	Temperature (K)
V	Volume (mL)
w	Constant - Exponent used in correlation
β	Coefficient of thermal expansion (K^{-1})
ΔH	Latent heat of fusion (J g^{-1})
$\phi 1$	Inner cavity diameter (mm)
$\phi 2$	Internal diameter of annular space (mm)
$\phi 3$	External diameter of annular space (mm)
$\phi 4$	Internal diameter of insulation (mm)
$\phi 5$	External diameter of insulation (mm)
$\phi 6$	External diameter of TESU (mm)
ε	Emissivity coefficient
σ	Stefan-Boltzmann Constant (W m^{-2} K^{-4})
σ^2	Variance
μ	Viscosity

Subscripts

air	Air
ext	External
H2O	Water
ins	Insulation
int	Internal
l	liquid
PCM	Phase change material
SA-PA	Unencapsulated stearic acid-palmitic acid mixture
SA-PA/TiO2	Stearic acid-palmitic acid mixture nanoencapsulated with titanium dioxide shell
s	solid
s-l	Solid-liquid phase change
steel	steel
t	Time
w	Wall
∞	Room

Herein, the studies were carried out with a mixture of commercial stearic and palmitic acid in a ratio of 89:11. The fatty acid mixture was evaluated as phase-change material using a device designed and built as a small scale model of a domestic water heater. Furthermore, in order to compare the performance of the proposed PCM with others reported in literature, a heat transfer model coupled with simple crystallization kinetics was developed.

A disadvantage common to all organic PCMs is their low thermal conductivity and, therefore, a low heat transfer coefficient. In order to improve the heat transfer coefficient, dispersion of conductive nanomaterials such as alumina or metallic nanoparticles in the organic phase, as well as encapsulation of the organic PCM with an inorganic conductive material were reported [16,18–24]. The last strategy is especially attractive because the capsule not only improves the heat transfer coefficient, but also protects the PCM from external conditions, extending its usable life and prevents dispersion of the material when melting [25–27].

In order to improve its thermal conductivity, the fatty acid mixture used in this work was encapsulated with titanium dioxide and the nanocapsules were subject to physical, morphological and thermal studies. To estimate the energy savings, the nanocapsules were incorporated into the device mentioned above and thermodynamic calculations were carried out.

Experimental

Chemicals

Stearic (SA, purity percent ≥ 95%) and palmitic acid (PA, purity percent ≥ 98%,) were purchased from Sigma-Aldrich. Sodium dodecyl sulfate (SDS) was purchased from Merck. Titanium (IV) butoxide (reagent grade) ($Ti(BuO)_4$) used as TiO_2 precursor for the formation of the PCM shell was purchased from Sigma-Aldrich. Anhydrous ethanol (99.5%, Sigma-Aldrich) and milli-Q water (18 MΩ quality) were used as solvents. Hydrochloric acid was purchased from Merck.

Preparation of the PCM

Preparation of the SA-PA mixture (synthetic soybean oil derivative)

In a beaker, 22.25 g of SA and 2.75 g of PA were added (ratio 89/11 w/w) and the mixture was melted to a clear liquid at 80 °C. The melted sample was stirred for 10 min at 80 °C to ensure the entire homogeneity of the mixture, and then cooled with continuous stirring to room temperature until complete solidification. The melting point of the mixture (SA-PA) was in agreement with the proposed application (60–69 °C).

Preparation of nanoencapsulated SA-PA with TiO_2 shell

SA-PA/TiO_2 nanocapsules were synthesized as was previously described [10]. Briefly, an emulsion was prepared by mixing SA-PA (25 g), SDS (3.5 g) and distilled water (300 mL). The pH was adjusted to 2–3 by adding HCl (0.1 M). In a separate flask, the precursor was prepared by adding 25 g of $Ti(BuO)_4$ to 80 mL of absolute ethanol. Nanocapsules formation was achieved by adding the precursor solution into the SA-PA emulsion drop by drop. After 2 h, the mixture was cooled to room temperature and the resulting white powder was separated by centrifugation, washed twice with distilled water and ethanol, and dried at 50 °C in a vacuum oven for 24 h.

Analytical methods

The chemical structural analyses of SA-PA/TiO_2 nanocapsules were performed on a Fourier Transform Infrared Spectrometer (*FT*-IR Thermo Scientific Nicolet 6700) using KBr pellets and the spectra was recorded from 400 to 4000 cm^{-1}. Morphological studies were carried

out by scanning electron microscopy (SEM-Carl Zeiss NTS, Supra 4) and transmission electron microscopy (TEM-Philips EM 301). The thermal properties were studied by differential scanning calorimeter (DSC Q20 TA Instruments-RSC 90). A heating scan of 10 °C min^{-1} from 20 °C to 120 °C was applied under a nitrogen stream at a flow rate of 50 mL min^{-1}. Then, the sample was cooled at 5 °C min^{-1} from 120 to 20 °C. The nanocapsules thermal stability was studied by thermogravimetric analyses (TGA Shimadzu TGA-51) from room temperature to 800 °C with a linear heating rate of 10 °C min^{-1} under a constant stream of nitrogen at a flow rate of 20 mL min^{-1}.

Thermal analyses

Design and construction of the thermal energy storage unit

A small-scale device (Thermal Energy Storage Unit (TESU)) was designed taking into account the cylindrical geometry of commercial water heaters with a high aspect ratio, which was chosen considering that the heat flux is mainly in the radial direction [28,29]. The design included two concentric cavities in a vertical disposition: the inner cavity planned to contain PCMs and the annular space to contain water, as shown in Fig. 1.

Based on the design described above, a prototype was built to carry out the thermal studies. The prototype was constructed in stainless steel 304 and the exterior walls, as well as the top and bottom of the device, were covered with glass wool as insulating material (Fig. 2, Table 1).

Given that the thermal storage unit is conceived to emulate a standard water heater, it is necessary to maintain the exterior wall at a safe temperature level for the end-user. To this end, the insulation thickness was calculated so that the wall temperature is always below 45 °C, which is considered a safe temperature [29,30].

Experimental set-up and procedure

Type k thermocouples (ETI) connected to a data logger (OnSet, Hobo) were used for the temperature measurement. Four temperature sensors were used to register the temperature of: the PCM (T_{PCM}), the water (T_{H2O}), the external wall (T_w) and the room (T_∞). Their radial positions are shown schematically in Fig. 3. All four thermocouples were vertically placed at half the height of the TESU device.

For the thermal experiments, the inner cavity of the TESU was filled with unencapsulated SA-PA mixture (15 g) and the annular space with hot water (66 g). The experiments started when the water temperature was at 80 °C and, after that, temperatures were recorded for every minute until reaching 40 °C.

In order to analyze the effect of the nanoencapsulation in thermal transport properties, further experiments were carried out in the same way, but filling the inner cavity with the nanoencapsulated SA-PA/TiO_2 (8.11 g). Also, blank experiments with the inner cavity empty were carried out.

Model development

In order to compare the performance of the proposed PCM with others reported in literature, a heat transfer model coupled with a simple crystallization kinetics was developed to reproduce the experimental cooling curves when the inner tube of TESU was filled with the unencapsulated SA-PA mixture.

The model considers 1D radial heat transfer in cylindrical coordinates, discretizing the time evolution in one-minute intervals. Two heat balances were considered at each time point: one between the PCM phase and the annular space filled with water, and another one between the latter and the outside air. A global stationary balance between the PCM phase and room air is not strictly possible in this case since both the PCM and water were heated initially to 80 °C.

Since the top and bottom of the device are well insulated, and the surface of the inner tubes is more than 28 times that of the lids, axial heat flow is expected to be negligible. Thus, only radial flow is considered. The heat balances were divided in three stages according to the state of the PCM (liquid, solid–liquid or solid). The heat balance in the liquid PCM phase in an interval Δt, using an Euler-forward method is:

$$m_{PCM} C_{P_{PCM_l}} (T_{PCM(t+\Delta t)} - T_{PCM(t)}) = -\dot{Q}_{l\_PCM(t)} \Delta t \quad (1)$$

where $\dot{Q}_{l\_PCM}$ is the heat lost by this phase and is computed, in cylindrical coordinates, as:

$$\dot{Q}_{l\_PCM(t)} = \frac{2\pi L_{int} (T_{1(t)} - T_{2(t)})}{r_1 h_1 + \frac{ln\left(\frac{r_2}{r_1}\right)}{k_{steel}} + \frac{ln\left(\frac{(r_2+r_3)}{2r_2}\right)}{k_{H2O}}} \quad (2)$$

The use of a heat transfer coefficient, h_1, is used to avoid the singularity at $r = 0$ in the inner cavity even though heat is probably transferred by conduction in this system. The heat balance for the aqueous phase assumes that the heat lost by the PCM is gained by the water:

$$m_{H2O} C_{P\_H2O} (T_{H2O(t+\Delta t)} - T_{H2O(t)}) = (\dot{Q}_{l\_PCM(t)} - \dot{Q}_{l\_H2O(t)}) \Delta t \quad (3)$$

Heat lost by the water phase is computed similarly to Eq. (2) without the need to introduce any heat transfer coefficients, assuming that heat is transported by conduction in the liquid phase:

$$\dot{Q}_{l\_H2O(t)} = \frac{2\pi L_{int} (T_{H2O(t)} - T_{w(t)})}{\frac{ln\left(\frac{2r_3}{(r_2+r_3)}\right)}{k_{H_2O}} + \frac{ln\left(\frac{r_4}{r_3}\right)}{k_{steel}} + \frac{ln\left(\frac{r_5}{r_4}\right)}{k_{ins}} + \frac{ln\left(\frac{r_6}{r_5}\right)}{k_{steel}}} \quad (4)$$

In turn, the wall temperature T_w is calculated under the steady-state assumption that the heat lost by the water phase is equal to the one transferred between the wall and the outside air, which is assumed to be at a bulk "infinite" temperature T_∞:

$$\frac{T_{H2O(t)} - T_{w(t)}}{\frac{ln\left(\frac{r_4}{r_3}\right)}{k_{steel}} + \frac{ln\left(\frac{r_5}{r_4}\right)}{k_{ins}} + \frac{ln\left(\frac{r_6}{r_5}\right)}{k_{steel}}} = r_6 (h_{ext} (T_{w(t)} - T_\infty) + \sigma\varepsilon ({T_{w(t)}}^4 - {T_\infty}^4)) \quad (5)$$

Eq. (5) is solved for T_w for known values of T_{H2O} (calculated with Eq. (3)), and T_∞, which is taken as the average of the measured valued since it is practically constant throughout the experiments.

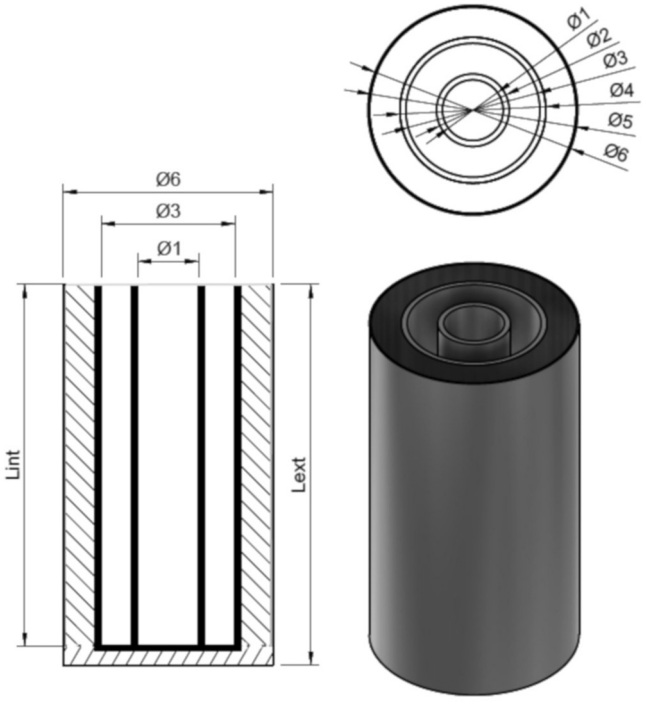

Fig. 1. Schematic diagram of the Thermal Energy Storage Unit.

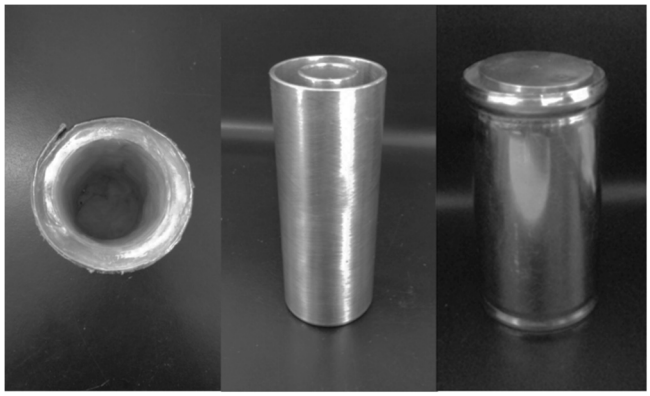

Fig. 2. Photos of the TESU prototype.

Table 1
Geometrical dimensions of the TESU.

Inner Tube Diameter	$\phi 1$	15.9	mm
Annular Space – Internal Diameter	$\phi 2$	19.1	mm
Annular Space – External Diameter	$\phi 3$	35.1	mm
Insulation – Internal Diameter	$\phi 4$	38.3	mm
Insulation – External Diameter	$\phi 5$	54.1	mm
External Diameter	$\phi 6$	55.1	mm
Internal Height	L_{int}	100	mm
External Height	L_{ext}	110	mm
Wall Thickness	e_w	1.57	mm
Insulation Thickness	e_{ins}	8.7	mm
Inner Tube Volume	V_{PCM}	19.93	mL
Annular Space Volume	V_{H2O}	68.47	mL

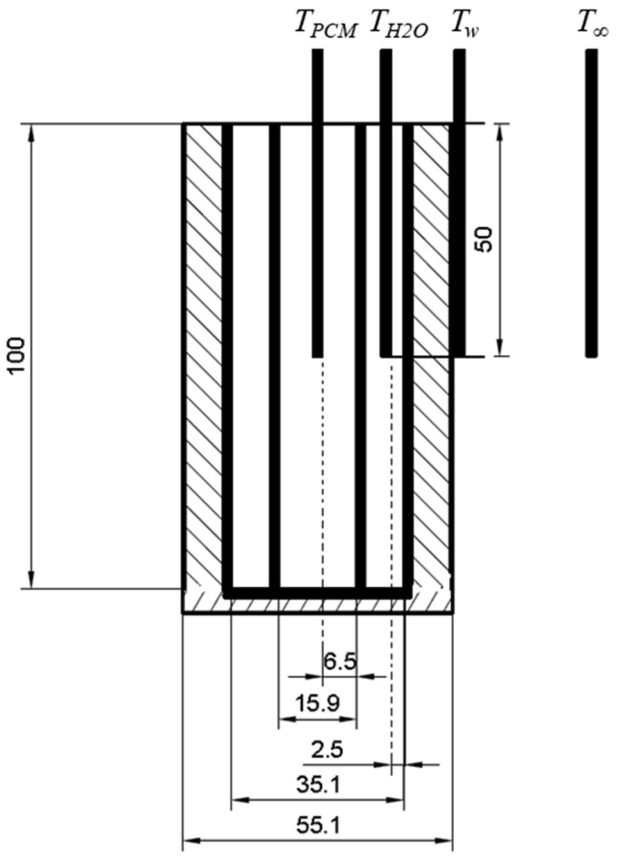

Fig. 3. Arrangement of thermocouples in the TESU.

Eqs. (1)–(5) are solved for each one-minute interval with the initial values of T_{PCM} and T_{H2O} corresponding to the measurements at $t = 0$, until the PCM phase reaches the crystallization temperature. From that point onwards, the heat balance of both the PCM and the aqueous phase must contemplate the heat released by the crystallization process. During this period, the following is assumed: i) the solidification mechanism is by nucleation and growth, ii) the growing crystals are located throughout the PCM volume, not necessarily growing from the outer wall in, iii) heat generated in the process is transferred to both the PCM and the water phases in a ratio that may be adjusted, and iv) the liquid and the solid phases in the inner cavity are at the same temperature for each time point.

With these hypotheses, the heat balance in the PCM phase is:

$$(m_{PCM\_l(t)}C_{P\_PCM\_l} + m_{PCM\_s(t)}C_{P\_PCM\_s})(T_{PCM(t+\Delta t)} - T_{PCM(t)}) = Q_{g\_PCM(t)} - \dot{Q}_{l\_PCM(t)}\Delta t \quad (6)$$

with:

$$Q_{g\_PCM(t)} = \alpha(m_{PCM\_s(t)} - m_{PCM\_s(t-\Delta t)})\Delta\widehat{H}_m \quad (7)$$

$$\dot{Q}_{l\_PCM(t)} = U_{(t)}2\pi r_1 L_{int}(T_{PCM(t)} - T_{H2O(t)}) \quad (8)$$

Eq. (7) represents the heat gained by the solidified PCM mass in a time interval Δt, due to the solidification process, with α being an adjustable parameter. The overall heat transfer coefficient in Eq. (8), $U_{(t)}$, shall depend on the amount of solidified material, and in this work it is suggested to be of the form:

$$U_{(t)} = \frac{1}{a\ln(\sqrt{m_{PCM\_s(t)}} + b) + c} \quad (9)$$

The spirit of this functionality is to keep the analogy between a standard heat transfer coefficient by conduction, which would depend on the radial position at which the solid phase would begin if it were perfectly separated from the liquid phase. In turn, this radius would depend on the square root of the solidified mass, given the annular geometry of the problem, hence the suggested form. Constants *a*, *b* and *c* are considered adjustable parameters of the model. $m_{PCM\_s(t)}$ is expressed in kg.

The heat balance for the water phase in this solidification process is:

$$m_{H2O}C_{P\_H2O}(T_{H2O(t+\Delta t)} - T_{H2O(t)}) = (\dot{Q}_{l\_PCM(t)}\Delta t + (1-\alpha)(m_{PCM\_s(t)} - m_{PCM\_s(t-\Delta t)})\Delta\widehat{H}_m - \dot{Q}_{l\_H2O(t)})\Delta t \quad (10)$$

The crystallization process is modeled with the traditional Avrami equation, which showed good results with lipids [31]:

$$m_{PCM\_s(t)} = m_{PCM}(1 - e^{-K(t-\tau)^n}) \quad (11)$$

where *K* and *n* are adjustable parameters and τ is the time at which the solidification process begins. Both t and τ are expressed in minutes.

Finally, for the PCM in solid state, the heat transfer model is computed similarly to the one considered for the liquid state (Eqs. (1)–(5)) but using the physical properties of the solid material.

Results and discussion

Measurements of cooling curves using SA-PA mixture – Model adjustment

In order to study the performance of the proposed PCM, cooling curves were constructed from 80 to 40 °C filling the inner cavity of the device described in the Experimental Section with SA-PA mixture and comparing the results with that obtained from a blank (the inner cavity empty). As it can be seen in the Fig. 4, during the cristalization process the latent heat stored by the PCM is released, increasing the temperature of the PCM phase, and the thermal energy is transferred from the PCM to the water.

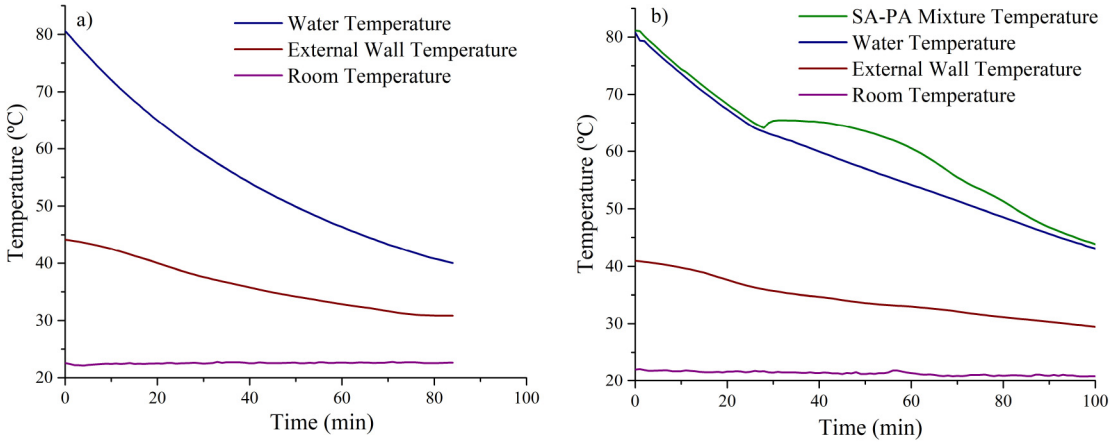

Fig. 4. Cooling curves of TESU: a) Blank; b) Filled with SA-PA Mixture.

In order to compare the proposed PCM with others reported in literature, the cooling curves of the device filled with SA-PA mixture were predicted with the simple heat transfer-crystallization model described in Model Development Section using the thermophysical properties shown in Table 2. Results are shown in Fig. 5, where a very good agreement is observed (RMSE: T_{PCM} = 1.0 °C; T_{H2O} = 0.7 °C; T_w = 0.4 °C; maximum E% = 2.4%). The values of the adjusted parameters are summarized in Table 3.

Taking into account the good fit between the experimental data and the analytical curves, the adjusted model was used to compare the proposed PCM with the theoretical performance of other organic PCMs reported in literature, under the conditions of this work. The cooling curves of these materials were then calculated with the boundary and initial conditions of the experiment. This procedure makes it possible to compare the materials in terms of their thermal performance as if they had been used in the TESU of this work. Results are shown in Fig. 6, where the time evolution of the water temperature is plotted for all the considered materials. The time required to reach 40 °C is listed in Table 4 for each case.

As it can be seen, the performance of the proposed PCM was similar and even better than other reported, but with the great advantage that it can be obtained from soybean oil, an environmentally friendly, renewable and abundant source.

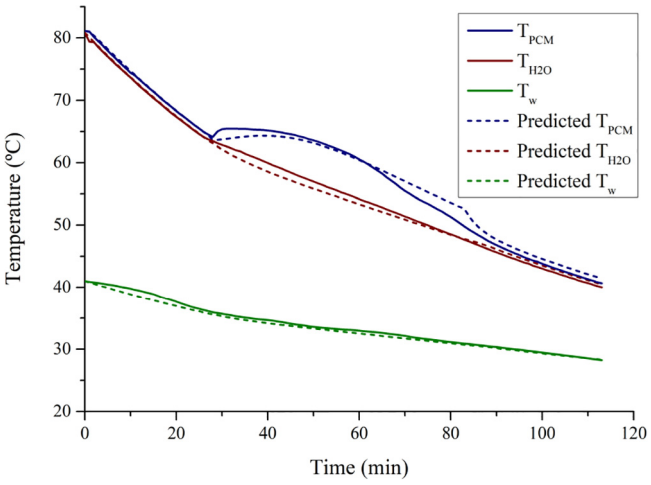

Fig. 5. Experimental and predicted (dashed lines) cooling curves (RMSE: T_{PCM} = 1.0 °C; T_{H2O} = 0.7 °C; T_w = 0.4 °C; maximum E% = 2.4%).

Table 3
Values of the adjusted parameters.

Parameter	Value	Unit
h_1	150	$W{\cdot}m^{-2}{\cdot}K^{-1}$
α	0.59	–
a	0.3666	$m^2{\cdot}K{\cdot}W^{-1}$
b	1.022	–
c	$1.04{\cdot}10^{-5}$	$m^2{\cdot}K{\cdot}W^{-1}$
K	0.0089	–
n	1.5086	–

Nanoencapsulation of the SA-PA mixture

The results described above were good enough to encourage further studies geared toward the improvement of the heat transfer coefficient and the stability of the PCM. With this aim, SA-PA mixture was encapsulated with titanium dioxide and the nanocapsules were characterized morphologically, structurally and thermally.

The morphological studies were carried out by SEM and TEM. Fig. 7a, b) shows the spherical shape of the capsules as well as their smooth and compact surface. From SEM images, the particle size distribution was estimated in the range of 80–100 nm. This result was in agreement with the TEM images (Fig. 7c, d) that showed agglomerates of nanoparticles of similar size that those observed by SEM.

The *FT*-IR spectra of TiO_2, unencapsulated SA-PA mixture, and nanoencapsulated SA-PA/TiO_2 particles, are shown in Fig. 8. The spectrum of the fatty acid mixture showed in the 2500–3500 cm^{-1} range, the characteristic profile of the carboxylic acids. In this range of wavenumber, the stretching vibrations of $–CH_3$ and $–CH_2$ appear at 2918 y

Table 2
Thermophysical properties.

ΔH_{SA-PA}	187.0 J g^{-1} (SD 0.19 J g^{-1}) (calculated from DSC, see section 3.2)
$c_{P\_SA-PA\_liquid}$	2.73 J g^{-1} K^{-1} (SD 0.1 J g^{-1} K^{-1}) (calculated from DSC, see section 3.2)
$c_{P\_SA-PA\_solid}$	2.70 J g^{-1} K^{-1} (SD 0.24 J g^{-1} K^{-1}) (calculated from DSC, see section 3.2)
k_{SA-PA_liquid}	0.18 W m^{-1} K^{-1} [32]
k_{SA-PA_solid}	0.30 W m^{-1} K^{-1} [33]
k_{ins}	0.044 W m^{-1} K^{-1} (SD 0.0084 W m^{-1} K^{-1})

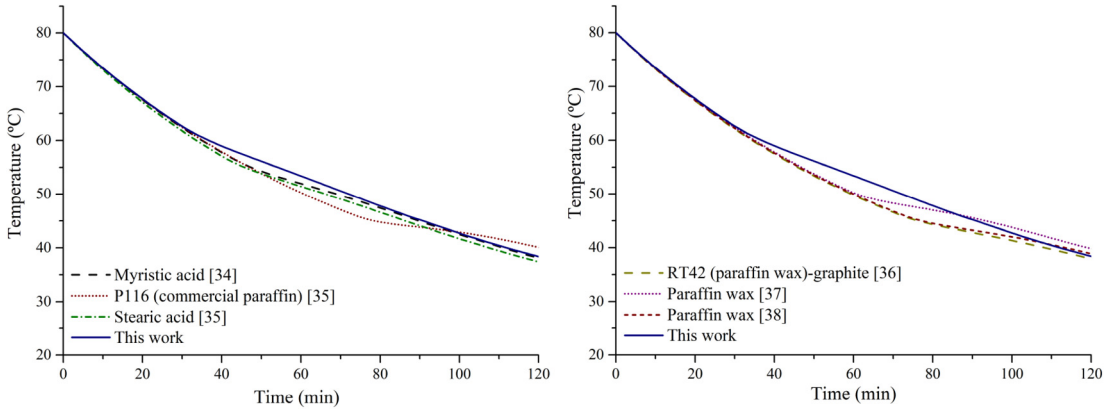

Fig. 6. Comparison of cooling curves between different PCMs from literature with the one used in this work.

Table 4
Comparison of the time required for the water to reach 40 °C.

PCM	Time (min)	Reference
Myristic acid	110	[34]
P116 (commercial paraffin)	120	[35]
Stearic acid	108	[35]
RT42 (paraffin wax)-graphite	109	[36]
Paraffin wax	118	[37]
Paraffin wax	113	[38]
SA-PA 89:11	113	This work

2850 cm^{-1} overlapped by the stretching vibration of the OH. The peak at 1701 cm^{-1} corresponds to the C═O stretching vibration and the signal at 941 cm^{-1} was assigned to the out of plane bending vibration of the −OH functional group. Besides, signal at 710 cm^{-1} was assigned to the bending vibration of the methylene groups.

On the other hand, in the TiO_2 spectrum, signals centered at 3400 and 1630 cm^{-1} were assigned to the water absorbed in the material, since the absorptions peaks of the titanium oxide appear in the far IR region [39].

The spectrum of the encapsulated SA-PA mixture was similar to that of the unencapsulated PCM, indicating that the chemical structure of fatty acids remains unchanged after the encapsulation process.

Thermal stability was analyzed by TGA (Fig. 9a). The TGA curves did not show a significant increased on thermal stability of the encapsulated PCM with respect to the unencapsulated mixture, as was previously reported for similar systems [15,16]. Besides, no residue remains at the end of the analysis of the unencapsulated SA-PA mixture while, in the case of encapsulated particles, the analysis left a 32% of residue from the inorganic shell. On the other hand, in the unencapsulated SA-PA curve only one step of degradation was observed,

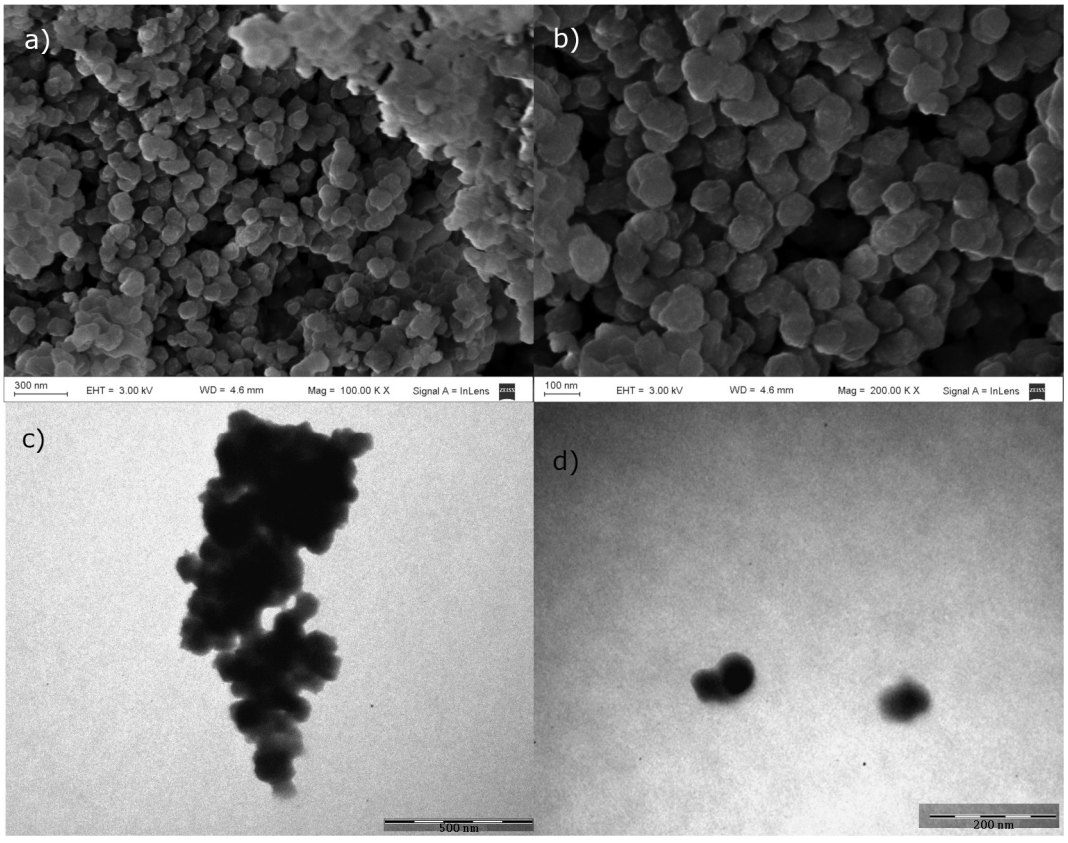

Fig. 7. a-b) SEM and c-d) TEM images of nanoencapsulated SA-PA/TiO_2.

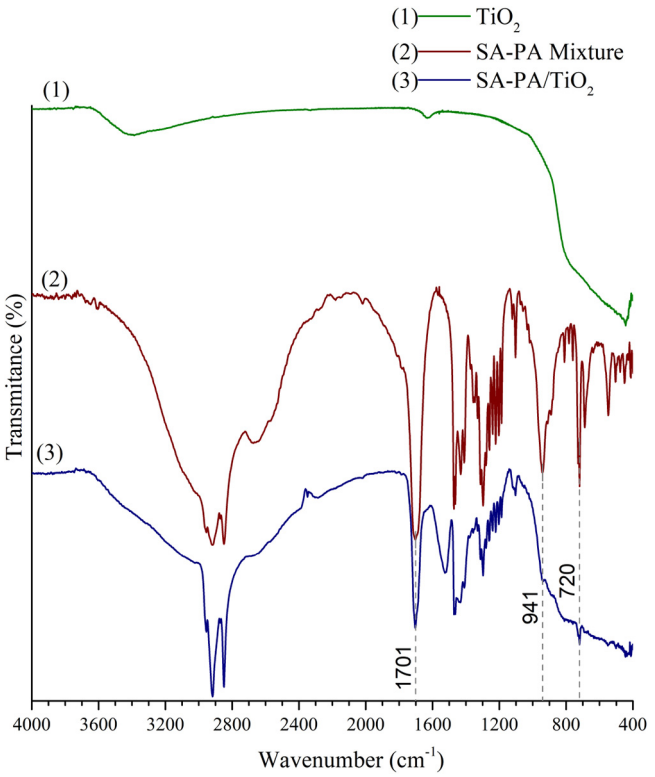

Fig. 8. FT-IR spectra of the TiO_2, unencapsulated SA-PA mixture and nanoencapsulated SA-PA/TiO_2.

while, in the case of the encapsulated particles, a second step over a temperature range of 400–600 °C was also observed. This second step was assigned by Cao et al. [10] to the thermal degradation of the TiO_2 gel and the crystal transition of TiO_2 from the amorphous state to anatase phase.

DSC analyses were also carried out and the melting points observed in the DSC curves (Fig. 9b), both for the unencapsulated SA-PA mixture and for the nanocapsules, were in agreement with the proposed application (60–69 °C).

The latent heats were determined by integrating the melting peaks and resulted to be 187.0 (SD 0.19) and 91.87 (SD 0.092) J g^{-1} for the unencapsulated and encapsulated PCM, respectively [40]. The encapsulation ratio (%*R*) of the PCM was calculated from Eq. (12), as was described elsewhere, and resulted to be 49.1% [10].

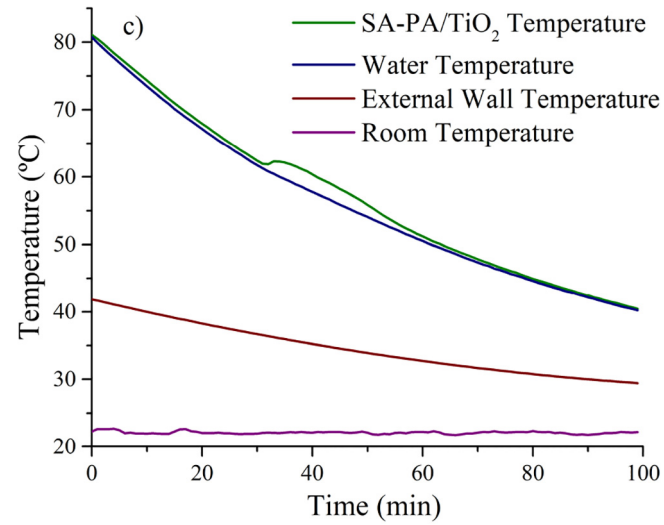

Fig. 10. Cooling curves of TESU filled with SA-PA/TiO_2.

$$\%R = \frac{\Delta H_{SA-PA/TiO2}}{\Delta H_{SA-PA}} \times 100\% \quad (12)$$

Measurements of cooling curves using SA-PA/TiO_2 – Thermodynamic and heat transfer calculations

Once the nanocapsules were obtained and characterized, cooling curves were performed in the same condition that were used for the unencapsulated mixture (Fig. 10).

Thermodynamic and heat transfer calculations were performed taking into account all time points of the cooling curves. The heat flux through the TESU was calculated using the temperature of the external wall and the room temperature and considering that the total heat transfer between the surface and the surroundings includes a convective and a radiant component (Eq. (13)) [28]. The convective heat transfer coefficient was calculated using the Nusselt-Rayleigh correlations for natural convection [29].

$$\dot{Q} = \dot{Q}_{conv} + \dot{Q}_{rad} = h_{air} A_{ext} (T_w - T_\infty) + \varepsilon\sigma A_{ext} (T_w^4 - T_\infty^4) \quad (13)$$

The heat flux obtained above was replaced in the equation of heat transfer through the insulation to calculate the temperature of the internal wall (Eqs. (14) and (15)). An excellent agreement was observed between the experimental and the calculated cooling curves in Fig. 11. Considering that the convective heat transfer coefficient of water phase should be much higher than the insulation heat transfer coefficient, the

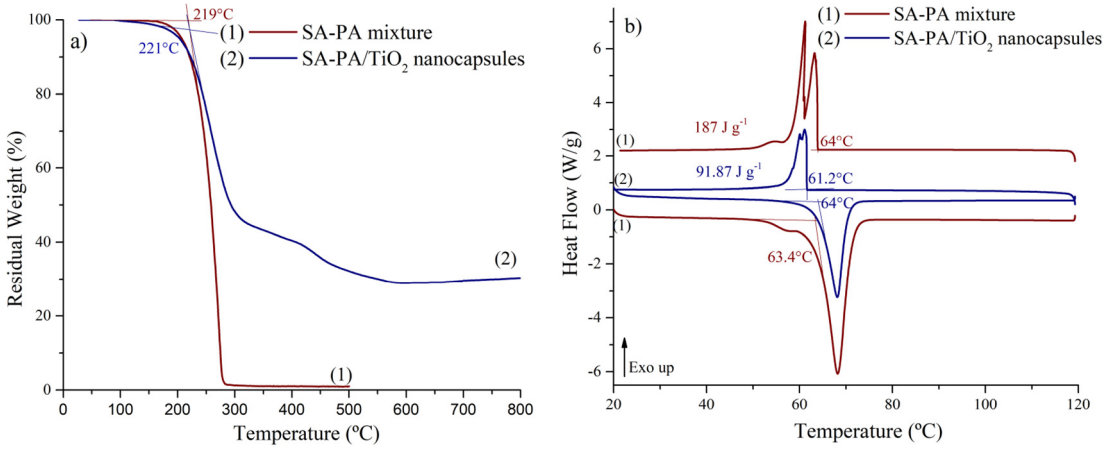

Fig. 9. a) TGA and b) DSC curves of unencapsulated SA-PA mixture and SA-PA/TiO_2 nanocapsules.

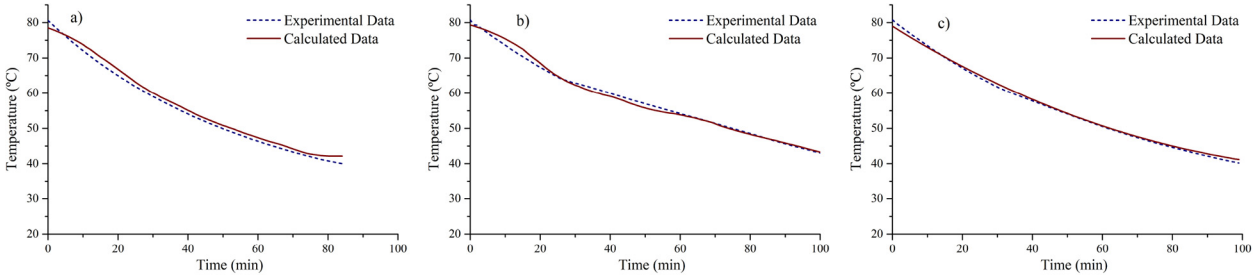

Fig. 11. Comparison of the calculated and experimental water temperature of: a) Blank; b) Unencapsulated SA-PA Mixture; c) SA-PA/TiO_2 nanocapsules.

temperature of the internal wall must be almost the same than the water temperature [28]. Therefore, this result showed that the correlations chosen for the calculations are representative of the system.

$$T_{w\_int} = T_w + \dot{Q}R_{ins} \tag{14}$$

$$R_{ins} = \frac{\ln\left(\frac{r_{ext_{ins}}}{r_{int_{ins}}}\right)}{2\pi L_{ext} k_{ins}} \tag{15}$$

The presence of the TiO_2 shell should enhance the heat transfer coefficient of the PCM due to its higher thermal conductivity. To confirm this, the thermal resistance to the heat flux was calculated in the PCM phase (Eq. (16)) [28]. The average thermal resistance for the fatty acids mixture resulted in 1.52 °C W^{-1} (SD 0.101 °C W^{-1}), while that of the nanoencapsulated PCM was 0.47 °C W^{-1} (SD 0.099 °C W^{-1}). That means that the TiO_2 shell reduced by about 70% the PCM thermal resistance.

$$R_{PCM} = \frac{T_{PCM} - T_{H2O}}{\dot{Q}} \tag{16}$$

Furthermore, thermal energy storage capacity studies were carried out and, taking into account the improvement in the thermal conductivity caused by the titanium dioxide shell, only the results with the encapsulated PCM are presented.

The thermal energy stored in the system at the beginning of the experiment (Eqs. (17)–(21)) was in agreement with the total amount of heat transferred from the device to the environment (Table 5), calculated as the integral of the heat flux over time (Eq. (18)) [28].

$$Q_{transferred} = \int_0^t \dot{Q}dt \tag{17}$$

$$Q_{stored} = Q_{H2O} + Q_{PCM} \tag{18}$$

$$Q_{H2O} = m_{H_2O} c_{P\_H2O}(T_{t=0} - T_t) \tag{19}$$

$$Q_{PCM} = m_{PCM}\%Rc_{P\_PCM\_l}(T_{t=0} - T_{s-l}) + m_{PCM}\%R\Delta H_{SA-PA} + m_{PCM}\% Rc_{P\_PCM\_s}(T_{s-l} - T_t) + m_{PCM}(1 - \%R)c_{P\_TiO2}(T_{t=0} - T_t) \tag{20}$$

$$E\% = \frac{Q_{transferred} - Q_{stored}}{(Q_{transferred} + Q_{stored})/2} \times 100\% \tag{21}$$

Then, the calculated thermal energy stored in the TESU filled with PCM was 10.6% higher respect to the blank, and the total cooling time of the water was increasead by over 18% thanks to the encapsulated PCM.

The results are good enough to encourage future scaling-up studies in order to evaluate the incorporation of the encapsulated PCM prepared in this work in a solar water heater.

Conclusions

The present paper proposes the use of soybean oil derivatives, which comes from an environmentally friendly, renewable and abundant source, as phase change materials. In particular, in this work, the experiments were carried out with a mixture of commercial palmitic and stearic acid in the proportion that would be obtained, on average, by soybean oil hydrolisis followed by hydrogenation. In order to perform thermal studies, a device simulating a commercial water heater was designed and constructed. A heat transfer model was developed to compare the performance of the proposed PCM with other materials reported in literature that have well-known disadvantages in terms of flammability, renewability, abundance and environmental care. Results showed that its performance, measured in terms of is heat storage capacity, is as good as theirs.

In order to improve the heat transfer coefficient as well as the stability of the PCM, the fatty acid mixture was encapsulated by a TiO_2 shell and the nanocapsules were characterized physical, thermal and morphologically.

Besides, comparative studies between encapsulated and unencapsulated PCM were carried out, observing a reduction of about 70% of the thermal resistance thanks to the TiO_2 shell. Finally, the calculated thermal energy stored in the device filled with nanoencapsulated PCM was 10.6% higher respect to the blank, and the total cooling time of the water was increasead by over 18% thanks to the PCM.

CRediT authorship contribution statement

Jorge Bergamo: Investigation, Methodology. **Ezequiel Rossi:** Formal analysis, Writing - original draft, Visualization. **Juan Martín Maffi:** Formal analysis, Software. **Laura De Angelis:** Investigation, Methodology, Funding acquisition, Writing - original draft. **María Inés Errea:** Conceptualization, Funding acquisition, Project administration, Writing - original draft, Writing - review & editing.

Declaration of Competing Interest

The authors declare that they have no known competing financial interests or personal relationships that could have appeared to influence the work reported in this paper.

Acknowledgments

The authors acknowledge Instituto Tecnológico de Buenos Aires (grant ID: ITBACyT35) for financial support. Ezequiel Rossi and Juan Martín Maffi have fellowships from CONICET.

Table 5
Results of the thermodynamics calculation from the experimental data.

	Blank	SA-PA/TiO_2 nanocapsules
$Q_{transferred}(J)$	11 251.2 (SD 8.5)	11 811.4 (SD 8.8)
$Q_{H_2O}(J)$	11 214.5 (SD 444.5)	11 214.5 (SD 482.6)
$Q_{PCM}(J)$	–	1191.8 (SD 82.0)
$Q_{stored}(J)$	11 214.5 (SD 444.5)	12 406.4 (SD 489.5)
$E\%$	0.33%	−4.91%

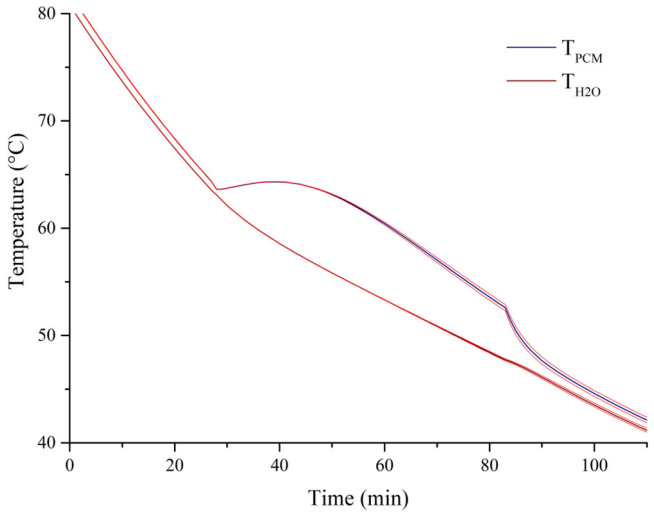

Fig. A1. Predicted cooling curves and their uncetainties.

Appendix A

In this appendix, the uncertain analysis is presented. First, the variation of the cooling curves calculated with the proposed model considering the variation of ΔH and c_p's (see Table 2) is presented. The red lines on Fig. A1 show the uncertainty of the predicted temperatures.

Besides, an error propagation analysis on Eqs. (13) to (22), considering the measurement uncertainties, was performed using Eqs. (A1) to (A23). Table A1 shows the uncertainties of all measured variables. Standard deviation of calculated parameters is shown throughout the article.

$$\sigma_{\%R}{}^2 = \frac{\sigma_{\Delta H_{SA-PA/TiO2}}{}^2}{\Delta H_{SA-PA}{}^2} + \frac{\Delta H_{SA-PA/TiO2}{}^2}{\Delta H_{SA-PA}{}^2}\cdot\sigma_{\Delta H_{SA-PA}}{}^2 \tag{A1}$$

$$\sigma_{\dot{Q}}{}^2 = \left(\frac{\delta\dot{Q}}{\delta h_{air}}\right)^2\cdot\sigma_{h_{air}}{}^2 + \left(\frac{\delta\dot{Q}}{\delta A_{ext}}\right)^2\cdot\sigma_{A_{ext}}{}^2 + \left(\frac{\delta\dot{Q}}{\delta T_w}\right)^2\cdot\sigma_{T_w}{}^2 + \left(\frac{\delta\dot{Q}}{\delta T_\infty}\right)^2\cdot\sigma_{T_\infty}{}^2 \tag{A2}$$

$$\frac{\delta\dot{Q}}{\delta h_{air}} = A_{ext}\cdot(T_w - T_\infty) \tag{A3}$$

$$\frac{\delta\dot{Q}}{\delta A_{ext}} = h_{air}\cdot(T_w - T_\infty) + \varepsilon\cdot\sigma\cdot(T_w{}^4 - T_\infty{}^4) \tag{A4}$$

$$\frac{\delta\dot{Q}}{\delta T_w} = h_{air}\cdot A_{ext} + 4\cdot\varepsilon\cdot\sigma\cdot A_{ext}\cdot T_w{}^3 \tag{A5}$$

$$\frac{\delta\dot{Q}}{\delta T_\infty} = -h_{air}\cdot A_{ext} - 4\cdot\varepsilon\cdot\sigma\cdot A_{ext}\cdot T_\infty{}^3 \tag{A6}$$

$$\sigma_{A_{ext}}{}^2 = \pi^2\cdot L_{ext}{}^2\cdot\sigma_{\phi 6}{}^2 + \pi^2\cdot\phi_6{}^2\cdot\sigma_{L_{ext}}{}^2 \tag{A7}$$

$$h_{air} = \frac{Nu\cdot k_{air}}{\phi_6} \tag{A8}$$

$$\sigma_{h_{air}}{}^2 = \frac{k_{air}}{\phi_6}\cdot\sigma_{Nu}{}^2 + \left(\frac{Nu\cdot k_{air}}{\phi_6{}^2}\right)^2\cdot\sigma_{\phi 6}{}^2 \tag{A9}$$

$$Nu = [[Nu_{COND}{}^n + (G\cdot\bar{c}_l\cdot Ra^{0.25})^n]^{w/n} + (\bar{c}_t\cdot Ra^{1/3})^w]^{1/w} \tag{A10}$$

$$\sigma_{Nu}{}^2 = \left(\frac{dNu}{dRa}\right)^2\cdot\sigma_{Ra}{}^2 \tag{A11}$$

Table A1
Uncertainty of the measurements.

	Measurement uncertainty
ϕ (mm)	0.1
L (mm)	1
T (K)	0.12
m (g)	0.5

$$\frac{dNu}{dRa} = \frac{1}{w}\cdot\left[\left(Nu_{COND}{}^{n} + \left(G\cdot\bar{c}_l\cdot Ra^{0.25}\right)^{n}\right)^{w/n} + \left(\bar{c}_t\cdot Ra^{1/3}\right)^{w}\right]^{\frac{1-w}{w}}\cdot$$
$$\left[\frac{w}{n}\cdot\left(Nu_{COND}{}^{n} + \left(G\cdot\bar{c}_l\cdot Ra^{0.25}\right)^{n}\right)^{\frac{w-n}{n}}\cdot G^{n}\cdot\bar{c}_l{}^{n}\cdot 0.25\cdot n\cdot Ra^{0.25\cdot n-1} + \bar{c}_t{}^{w}\cdot\frac{w}{3}\cdot Ra^{\frac{w}{3}-1}\right] \tag{A12}$$

$$Ra = \frac{g\cdot\beta\cdot(T_w - T_\infty)\cdot\phi_6{}^{3}\cdot \mathrm{Pr}}{\mu^2} \tag{A13}$$

$$\sigma_{Ra}{}^{2} = \left(\frac{g\cdot \mathrm{Pr}}{\mu^2}\right)^{2}\cdot\left[2\cdot\beta^2\cdot\phi_6{}^{6}\cdot\sigma_T{}^{2} + (T_w - T_\infty)^2\cdot\left(\phi_6{}^{6}\cdot\sigma_\beta{}^{2} + 9\cdot\beta^2\cdot\phi_6{}^{4}\cdot\sigma_{\phi 6}{}^{2}\right)\right] \tag{A14}$$

$$\beta = \frac{2}{T_w + T_\infty} \tag{A15}$$

$$\sigma_\beta{}^{2} = \frac{8}{(T_w - T_\infty)^4}\cdot\sigma_T{}^{2} \tag{A16}$$

$$\sigma^2_{T_{w\_\mathrm{int}}} = \sigma^2_{T_w} + R^2_{ins}\cdot\sigma^2_{\dot{Q}} + \dot{Q}\cdot\sigma^2_{R_{ins}} \tag{A17}$$

$$\sigma^2_{R_{ins}} = \left(\frac{1}{2\cdot\pi\cdot L_{ext}\cdot k_{ins}}\right)^2\cdot\left(\frac{\sigma^2_{r_{ext\_ins}}}{r^2_{ext_{ins}}} + \frac{\sigma^2_{r_{int\_ins}}}{r^2_{\mathrm{int}_{ins}}} + \left(\ln\frac{r_{ext_{ins}}}{r_{\mathrm{int}_{ins}}}\right)^2\cdot\frac{\sigma^2_{L_{ext}}}{L^2_{ext}} + \left(\ln\frac{r_{ext_{ins}}}{r_{\mathrm{int}_{ins}}}\right)^2\cdot\frac{\sigma^2_{k_{ins}}}{k^2_{ins}}\right) \tag{A18}$$

$$\sigma_{R_{PCM}}{}^{2} = \frac{2\cdot\sigma_T{}^{2}}{\dot{Q}^2} + \frac{(T_{PCM} - T_{H2O})^2\cdot\sigma_{\dot{Q}}{}^{2}}{\dot{Q}^4} \tag{A19}$$

$$\sigma_{Q_{transferred}}{}^{2} = \sum_{t=1}^{n}\left[60^2\cdot\left(\frac{\sigma_{\dot{Q}_t}{}^{2} + \sigma_{\dot{Q}_{t-1}}{}^{2}}{4}\right)\right] \tag{A20}$$

$$\sigma_{Q_{stored}}{}^{2} = \sigma_{Q_{H2O}}{}^{2} + \sigma_{Q_{PCM}}{}^{2} \tag{A21}$$

$$\sigma_{Q_{H2O}}{}^{2} = 2\cdot m_{H2O}{}^{2}\cdot c_{P\_H2O}{}^{2}\cdot\sigma_T{}^{2} + c_{P\_H2O}{}^{2}\cdot(T_{t=0} - T_t)^2\cdot\sigma_{m_{H2O}}{}^{2} \tag{A22}$$

$$\sigma_{Q_{PCM}}{}^{2} = m_{PCM}{}^{2}\cdot\sigma_{\Delta H_{SA-PA/TiO2}}{}^{2} + m_{PCM}{}^{2}\cdot\%R^2\cdot(T_{t=0} - T_{s-l})^2\cdot\sigma_{c_{P\_PCM\_l}}{}^{2} + m_{PCM}{}^{2}\cdot\%R^2\cdot(T_{s-l} - T_t)^2\cdot\sigma_{c_{P\_PCM\_s}}{}^{2} +$$
$$\left((1 - \%R)\cdot c_{P\_TiO2}\cdot(T_{t=0} - T_{s-l}) + \Delta H_{SA-PA/TiO2} + \%R\cdot(T_{t=0} - T_{s-l})\cdot c_{P\_PCM\_l} + \%R\cdot(T_{s-l} - T_t)\cdot c_{P\_PCM\_s}\right)^2\cdot\sigma_{m_{PCM}}{}^{2} +$$
$$\left(-m_{PCM}\cdot c_{P\_TiO2}\cdot(T_{t=0} - T_{s-l}) + m_{PCM}\cdot(T_{t=0} - T_{s-l})\cdot c_{P\_PCM\_l} + m_{PCM}\cdot(T_{s-l} - T_t)\cdot c_{P\_PCM\_s}\right)^2\cdot\sigma_{\%R}{}^{2} \tag{A23}$$

References

[1] Petroleum, B. BP Statical Review of World Energy. 2018 [cited 2019 04-23].

[2] Al-Hallaj, S. and Kiszynski, K., The Role of Renewable Energy in a Sustainable Energy Future, in Hybrid Hydrogen Systems: Stationary and Transportation Applications, S. Al-Hallaj and K. Kiszynski, Editors. 2011, Springer London: London. p. 1-8.

[3] Sheikholeslami M, Rezaeianjouybari B, Darzi M, Shafee A, Li Z, Nguyen TK. Application of nano-refrigerant for boiling heat transfer enhancement employing an experimental study. Int J Heat Mass Transf 2019;141:974–80. https://doi.org/10.1016/j.ijheatmasstransfer.2019.07.043.

[4] Sheikholeslami M, Jafaryar M, Shafee A, Babazadeh H. Acceleration of discharge process of clean energy storage unit with insertion of porous foam considering nanoparticle enhanced paraffin. J Cleaner Prod 2020;261:121206https://doi.org/10.1016/j.jclepro.2020.121206.

[5] Zhou D, Zhao CY, Tian Y. Review on thermal energy storage with phase change materials (PCMs) in building applications. Appl Energy 2012;92:593–605. https://doi.org/10.1016/j.apenergy.2011.08.025.

[6] Hasnain SM. Review on sustainable thermal energy storage technologies, Part I: heat storage materials and techniques. Energy Convers Manage 1998;39(11):1127–38. https://doi.org/10.1016/S0196-8904(98)00025-9.

[7] Akeiber H, Nejat P, Majid MZA, Wahid MA, Jomehzadeh F, Zeynali Famileh I, et al. A review on phase change material (PCM) for sustainable passive cooling in building envelopes. Renew Sustain Energy Rev 2016;60:1470–97. https://doi.org/10.1016/j.rser.2016.03.036.

[8] Praveen B, Suresh S, Pethurajan V. Heat transfer performance of graphene nanoplatelets laden micro-encapsulated PCM with polymer shell for thermal energy storage based heat sink. Appl Therm Eng 2019;156:237–49. https://doi.org/10.1016/j.applthermaleng.2019.04.072.

[9] Suppes GJ, Goff MJ, Lopes S. Latent heat characteristics of fatty acid derivatives pursuant phase change material applications. Chem Eng Sci 2003;58(9):1751–63. https://doi.org/10.1016/S0009-2509(03)00006-X.

[10] Cao L, Tang F, Fang G. Preparation and characteristics of microencapsulated palmitic acid with TiO2 shell as shape-stabilized thermal energy storage materials. Sol Energy Mater Sol Cells 2014;123:183–8. https://doi.org/10.1016/j.solmat.2014.01.023.

[11] Tang F, Cao L, Fang G. Preparation and thermal properties of stearic acid/titanium dioxide composites as shape-stabilized phase change materials for building thermal energy storage. Energy Build 2014;80:352–7. https://doi.org/10.1016/j.enbuild.2014.05.030.

[12] Şahan N, Paksoy H. Determining influences of SiO2 encapsulation on thermal energy storage properties of different phase change materials. Sol Energy Mater Sol Cells 2017;159:1–7. https://doi.org/10.1016/j.solmat.2016.08.030.

[13] Yi H, Zhan W, Zhao Y, Qu S, Wang W, Chen P, et al. A novel core-shell structural montmorillonite nanosheets/stearic acid composite PCM for great promotion of thermal energy storage properties. Sol Energy Mater Sol Cells 2019;192:57–64. https://doi.org/10.1016/j.solmat.2018.12.015.

[14] Xie B, Li C, Zhang B, Yang L, Xiao G, Chen J. Evaluation of stearic acid/coconut shell charcoal composite phase change thermal energy storage materials for tankless solar water heater. Energy Built Environ 2020;1(2):187–98. https://doi.org/10.1016/j.enbenv.2019.08.003.

[15] Tahan Latibari S, Mehrali M, Mehrali M, Afifi ABM, Mahlia TMI, Akhiani AR, et al. Facile synthesis and thermal performances of stearic acid/titania core/shell nanocapsules by sol–gel method. Energy 2015;85:635–44. https://doi.org/10.1016/j.energy.2015.04.008.

[16] Chen Z, Cao L, Shan F, Fang G. Preparation and characteristics of microencapsulated stearic acid as composite thermal energy storage material in buildings. Energy Build 2013;62:469–74. https://doi.org/10.1016/j.enbuild.2013.03.025.

[17] Woodfield, H.K. and Harwood, J.L., Oilseed Crops: Linseed, Rapeseed, Soybean, and Sunflower, in Encyclopedia of Applied Plant Sciences (Second Edition), B. Thomas, B.G. Murray, and D.J. Murphy, Editors. 2017, Academic Press: Oxford. p. 34-8.

[18] Ho CJ, Gao J. Preparation and thermophysical properties of nanoparticle-in-paraffin emulsion as phase change material. Int Commun Heat Mass Trans 2009;36(5):467–70. https://doi.org/10.1016/j.icheatmasstransfer.2009.01.015.

[19] Park SD, Lee SW, Kang S, Kim SM, Seo H, Bang IC. Effects of Al2O3/R-123 nanofluids containing C19H40 core–shell phase change materials on critical heat flux. Int J Heat Mass Transf 2012;55(23–24):7144–50. https://doi.org/10.1016/j.ijheatmasstransfer.2012.07.029.

[20] Sahan N, Paksoy HO. Thermal enhancement of paraffin as a phase change material with nanomagnetite. Sol Energy Mater Sol Cells 2014;126:56–61. https://doi.org/10.1016/j.solmat.2014.03.018.

[21] Pan L, Tao Q, Zhang S, Wang S, Zhang J, Wang S, et al. Preparation, characterization and thermal properties of micro-encapsulated phase change materials. Sol Energy Mater Sol Cells 2012;98:66–70. https://doi.org/10.1016/j.solmat.2011.09.020.

[22] Mehrali M, Latibari ST, Mehrali M, Metselaar HSC, Silakhori M. Shape-stabilized

phase change materials with high thermal conductivity based on paraffin/graphene oxide composite. Energy Convers Manage 2013;67:275–82. https://doi.org/10.1016/j.renene.2017.05.026.
[23] Yan Q, Liu C, Zhang J. Experimental study on thermal conductivity of composite phase change material of fatty acid and paraffin. Mater Res Express 2019. https://doi.org/10.1088/2053-1591/ab0d5e.
[24] Su W, Darkwa J, Kokogiannakis G. Nanosilicon dioxide hydrosol as surfactant for preparation of microencapsulated phase change materials for thermal energy storage in buildings. Int J Low-Carbon Technol 2018;13(4):301–10. https://doi.org/10.1093/ijlct/cty032.
[25] Huang X, Zhu C, Lin Y, Fang G. Thermal properties and applications of microencapsulated PCM for thermal energy storage: a review. Appl Therm Eng 2019;147:841–55. https://doi.org/10.1016/j.applthermaleng.2018.11.007.
[26] Su W, Li Y, Zhou T, Darkwa J, Kokogiannakis G, Li Z. Microencapsulation of Paraffin with Poly (Urea Methacrylate) Shell for Solar Water Heater. Energies 2019;12(18):3406.
[27] Su W, Darkwa J, Kokogiannakis G. Development of microencapsulated phase change material for solar thermal energy storage. Appl Therm Eng 2017;112:1205–12. https://doi.org/10.1016/j.applthermaleng.2016.11.009.
[28] Cengel Y. Heat and mass transfer: fundamentals and applications. McGraw-Hill Higher Education; 2014.
[29] Rohsenow WM, Hartnett JP, Cho YI. Handbook of heat transfer Vol. 3. New York: McGraw-Hill; 1998.
[30] Cao E. Transferencia de calor en ingeniería de procesos. Nueva librería; 2006.
[31] Narine SS, Humphrey KL, Bouzidi L. Modification of the Avrami model for application to the kinetics of the melt crystallization of lipids. J Am Oil Chem Soc 2006;83(11):913–21. https://doi.org/10.1007/s11746-006-5046-6.
[32] Sari A, Kaygusuz K. Thermal energy storage system using stearic acid as a phase change material. Sol Energy 2001;71(6):365–76. https://doi.org/10.1016/S0038-092X(01)00075-5.
[33] Bayram Ü, Aksöz S, Maraşlı N. Temperature dependency of thermal conductivity of solid phases for fatty acids. J Therm Anal Calorim 2014;118(1):311–21. https://doi.org/10.1007/s10973-014-3968-z.
[34] Wu S, Fang G. Dynamic performances of solar heat storage system with packed bed using myristic acid as phase change material. Energy Build 2011;43(5):1091–6. https://doi.org/10.1016/j.enbuild.2010.08.029.
[35] El Qarnia H. Numerical analysis of a coupled solar collector latent heat storage unit using various phase change materials for heating the water. Energy Convers Manage 2009;50(2):247–54. https://doi.org/10.1016/j.enconman.2008.09.038.
[36] Talmatsky E, Kribus A. PCM storage for solar DHW: an unfulfilled promise? Sol Energy 2008;82(10):861–9. https://doi.org/10.1016/j.solener.2008.04.003.
[37] Al-Hinti I, Al-Ghandoor A, Maaly A, Abu Naqeera I, Al-Khateeb Z, Al-Sheikh O. Experimental investigation on the use of water-phase change material storage in conventional solar water heating systems. Energy Convers Manage 2010;51(8):1735–40. https://doi.org/10.1016/j.enconman.2009.08.038.
[38] Reddy, K., Thermal modeling of PCM-based solar integrated collector storage water heating system. 2007. https://doi.org/10.1115/1.2770753.
[39] Yuan Y, Zhang N, Tao W, Cao X, He Y. Fatty acids as phase change materials: a review. Renew Sustain Energy Rev 2014;29:482–98. https://doi.org/10.1016/j.rser.2013.08.107.
[40] Su W, Gao L, Wang L, Zhi H. Calibration of differential scanning calorimeter (DSC) for thermal properties analysis of phase change material. J Therm Anal Calorim 2020. https://doi.org/10.1007/s10973-020-09470-9.